Robust High-Precision Option Pricing by Fourier Transforms: Contour Deformations and Double-Exponential Quadrature

Leif Andersen and Mark Lake*
Bank of America Merrill Lynch

First Version: April 2018 This version: September 2018

Abstract

While the idea of pricing options by Fourier methods has been around for more than two decades, the numerical evaluation of the necessary semi-infinite Fourier-style integrals remains a challenging problem. Existing methods in the literature frequently lack robustness, and in practice often yield disappointing precision, especially when the integrands are oscillatory or poorly dampened. In this paper we propose two new methods to evaluate these integrals, both relying on double-exponential quadrature. In the first, we use a carefully constructed contour deformation to dampen out Fourier oscillations in the integrand, followed by an application of either automatic or fixed-size double-exponential quadrature. In the second, we use a node-placement trick by T. Ooura to ensure that the integrand decays double-exponentially at all node points, even in the presence of oscillations. While both methods are generally applicable, for concreteness we mostly frame our development in the context of the popular (and tricky) Heston stochastic volatility model. As demonstrated by tests on hundred thousands of challenging model and option parameter configurations, our two schemes are efficient, accurate, and robust, and significantly outperform standard methods. For instance, in a challenging bulk test our recommended scheme (the DE-C method) is on average about 10 orders of magnitude more precise than standard adaptive Gauss-Lobatto quadrature, and is also far more robust.

*The authors wish to thank Dominique Bang, Rupert Brotherton-Ratcliffe and Mike Staunton for helpful suggestions. The opinions in this paper are those of the authors and do not necessarily represent those of their employer.

1 Introduction

1.1 Problem Statement and Literature Review

Consider a positive process $F(t)$ and define, for some fixed horizon $T > 0$ and any $u \in \mathbb{R}$, the characteristic function

$$\phi(u) = \mathbb{E}\left(e^{iuX(T)}\right), \quad X(T) \triangleq \ln\left(F(T)/F_0\right), \tag{1}$$

where i is the complex unit, $\mathbb{E}$ denotes expectation in some probability measure $\mathbb{P}$, and

$$F_0 = \mathbb{E}\left(F(T)\right).$$

Many important financial models have explicit formulas for the characteristic function of (the logarithm of) their underlying state variables. This includes, for instance, many asset price models based on Levy jump processes (e.g., [9], [14], [15], [16], [42]; surveys in [6] and [19]), as well as models based on affine or linear-quadratic jump-diffusion processes (e.g., [10], [16], [18], [21], [27], [56], and [58]). In addition, several important portfolio risk models produce explicit formulas for the characteristic function of portfolio returns (e.g., [26] and [54]).

For option pricing, and for risk and exposure calculations in general[1], it is often the case that we need to compute call-type expectations of the form

$$C(F_0, K) = \mathbb{E}\left((F(T) - K)^+\right) = \mathbb{E}\left(\left(F_0 e^{X(T)} - K\right)^+\right) \tag{2}$$

or, equivalently, of the put-type

$$P(F_0, K) = \mathbb{E}\left((K - F(T))^+\right) = K - F_0 + C(F_0, K).$$

The relationship between (2) and the characteristic function in (1) was first described by Heston in [27], using a direct application of the connection (e.g., [25]) between a characteristic function and a cumulative probability density function. The result in [27] is, for several reasons, suboptimal from a numerical perspective, and several authors have worked towards a re-statement in a form more suitable for computation. An important step was the introduction of a dampened Fourier transform in [13], followed by refinements and generalizations in [32], [36], [37], [38], and others. A modern formulation, which contains many early approaches as special cases, is given by[2]:

$$C(F_0, K) = R(\alpha, F_0, K) - \frac{F_0 e^{\alpha\omega}}{\pi} \int_0^\infty \mathrm{Re}\left\{e^{ix\omega} Q(x - i\alpha)\right\} dx, \tag{3}$$

where α is a real constant;

$$R(\alpha, F_0, K) = F_0 \cdot 1_{\alpha \le 0} - K \cdot 1_{\alpha \le -1} - \frac{1}{2}\left(F_0 \cdot 1_{\alpha=0} - K \cdot 1_{\alpha=-1}\right); \tag{4}$$

[1] The important conditional Value-at-Risk (CVaR) risk measure is of the form (2), as is the Expected Exposure metric used in credit risk applications.

[2] For a put we just use put-call parity: $P = C + (K - F)$

and

$$Q(z) \triangleq \frac{\phi(z-i)}{z(z-i)}, \quad \omega \triangleq \ln(F_0/K)\,. \tag{5}$$

We notice that (3) involves evaluation of $\phi(u)$ for complex-valued u. As is known from the theory of generalized Fourier transforms (see [61]), we cannot generally expect $\phi(u)$ to exist in the entire complex plane, so one needs to constrain the (otherwise arbitrary) real-valued dampening parameter α in (3) to a certain interval $(\alpha_{\min}, \alpha_{\max})$ for (3) to be well-defined; we discuss this in more detail in Sections 2 and 3, in the setting of a concrete model. A common, and reasonably robust, choice of α is $\alpha = -1/2$, but [39] shows that the behavior of the integrand can sometimes be improved by a more elaborate choice of α; see Section 3.2. We note in passing that the term R in (3) is best understood in the context of contour integration in the complex plane (see, e.g., Section 3), and originates with the residues of the simple poles at $z = i$ and $z = 0$ for the function Q.

While (3) is an improvement over earlier formulations, it is still challenging to evaluate numerically. Indeed, a numerical scheme must contend with several complications, including:

- a semi-infinite integration range (and resulting truncation errors of finite-interval quadrature schemes);
- the lack of analyticity of ϕ, and the existence of poles in Q;
- a sometimes highly oscillatory integrand, when the log-moneyness variable ω is numerically large and ϕ is slowly decaying (e.g., for small T).

Early numerical approaches focused primarily on applications of Fast Fourier Transform (FFT) and, later, fractional FFT (e.g., [13], [17], [32]), in part because of the potential of FFT to efficiently compute $C(F_0, K)$ for multiple values of the strike K. Following a demonstration in [31] of how caching techniques may improve the performance of direct integration methods, the literature has lately trended away from FFT methods towards higher-precision quadrature methods. Gaussian quadrature schemes are particularly popular in the literature (e.g., [30], [39], [55]), although some authors (e.g., [4] and [33]) use simpler schemes, such as Newton-Cotes or even trapezoidal integration. Adaptive versions of the various schemes are common. To deal with the semi-infinite integration range, some authors (e.g., [39]) suggest using a logarithmic variable transformation to map $[0, \infty)$ to the interval $(0, 1]$. Others (e.g., [5], [33], [36], [57]) use asymptotics to estimate a suitable upper truncation limit for the integral; this can be combined with an adaptive multi-domain integration approach, as in [65], for additional refinement.

One issue with all schemes discussed so far is that they are fundamentally not well-suited for oscillatory integrands and, in our experience, are often not robust across a wide array of model configurations, strikes K, and horizons T; see Section 6.2 for some typical results. The classical Filon-type technique for oscillatory integrands from the 1920's (see [23]) has recently been employed by [20] and [33], with reasonable results, at least

on relatively benign parameter configurations. Much more recent (and likely better-performing) methods for oscillatory integrands include the Levin collocation method (see [35]) and the method of numerical steepest descent (see [28]). The latter method is potentially very powerful, but is unfortunately not directly applicable to our problem, as it generally involves analyticity requirements on Q that are too strong. Nevertheless, we shall later see how elements of the contour-deformations central to numerical steepest descent can be applied to the problem at hand.

Finally, we should mention two specialized techniques that have received some attention in the literature. The first is based on an observation in [3] and involves the introduction of a control variate process with a characteristic function ϕ^* for which the expectation in (2) is known in closed form. If the closed form result is denoted $C^*(F_0, K)$, we may write

$$C(F_0, K) = C^*(F_0, K) - \frac{F_0 e^{\alpha\omega}}{\pi} \int_0^\infty \text{Re}\left\{ e^{ix\omega} \cdot \frac{\phi\left(x - i(1+\alpha)\right) - \phi^*\left(x - i(1+\alpha)\right)}{(x - i\alpha)\left(x - i(1+\alpha)\right)} \right\} dx,$$

where the hope is that the new integrand is better-behaved than the original one. The method has the advantage that the residue term R conveniently vanishes, and that the poles in the integrand can be made removable. In practice, the success of the method depends on an inspired choice of ϕ^*; for some examples of this, see [30]. We will not use the control variate method here, but it is likely that some applications might benefit from it.

A second specialized technique worth mention is the COS-algorithm, developed in [22]. The idea is here to represent the expectation in (2) through a Fourier-cosine expansion with a finite number of terms. Under some conditions, the convergence of the method will be given by the decay of the characteristic function. As the decay rate of characteristic functions tends to shrink as the horizon T is lowered, one would expect the basic COS-algorithm to be best-suited for larger value of T. See [33] and [34] for some numerical tests.

1.2 Organization of the Paper

Despite the many papers written on the topic, one often finds in real-life implementations that published techniques for computation of (3) lack robustness and frequently fail to produce the accuracy that coded tolerance levels promise. Often this originates with the fact that existing literature tends to run tests only a very limited, and often benign, set of model and contract parameters, and then declare victory based on too-narrow numerical evidence. Our goal here is to develop high-speed, high-precision methods that will produce accurate benchmark-quality values across a very wide parameter space. For concreteness, we will use the Heston model (see [27], [53]) throughout, both when developing our method and when testing its numerical performance. The Heston model provides a good way to showcase our results, as the model is well-known for having a number of thorny theoretical properties, and for being particularly tricky to implement numerically. For instance, the model is subject to moment explosions, potential

absorption of volatility at the origin, and a marked change in behavior (and theoretical properties) when the correlation is large and positive; see [4] and, especially, [29] for more details. To complicate matters further, the Heston characteristic function must be stated carefully to avoid branch-cut discontinuities, and has an infinite number of singularities none of which are known in closed form.

Our approach in this paper will be to attack the integral in (3) by two separate adaptations of the *double-exponential* (DE) quadrature method. Originally developed in Japan by Takahashi and Mori (see [60]), the DE method and its variants are increasingly popular in scientific applications[3], and have become known for simplicity and precision, converging exponentially fast for a wide range of integrands. Moreover, DE methods handle infinite integration ranges particularly well and often display remarkable robustness, being unfazed by end-point singularities, bad-behaving high-order derivatives, and overall lack of smoothness of the integrand. We shall touch upon some of these qualities, including the sense in which DE methods are optimal, in more detail later; we also recommend the surveys and comparative studies in, e.g., [8], [46], [47], [62], [64] for background. Applications of the DE method in Finance are so far relatively modest[4], perhaps because DE methods are not yet included in all popular integration software packages.

In its pure form, the DE method is not much better equipped than regular quadrature methods to handle the (potentially) highly oscillatory integrands in (3). We will present two distinct methods to deal with this problem. The first method (denoted DE-C) uses an analytical extension of the integral in (3) into the complex plane, along with a carefully chosen deformation of the integration path. The deformation, which is general and may be used with any quadrature rule, is designed to rapidly dampen oscillations from the Fourier oscillator $e^{iz\omega}$, while avoiding too-close passage of the singularities in ϕ. The second method (denoted DE-O), leans upon an ingenious trick by [48], [49], and [50] that ensures double-exponential decay of the integrand *at all quadrature points*, even in the presence of the Fourier oscillator.

The rest of the paper is organized as follows. In Section 2, we briefly introduce the Heston model and list the concrete characteristic function that we shall use as an integrand in (3). We also take the opportunity to establish certain asymptotics that shall be useful later. In Section 3, we describe how to improve the numerical properties of (3) by judicious changes of the integration path in the complex plane. In Sections 4 and 5, we then develop the DE-C and DE-O methods in the setting of the Heston model, in both adaptive and non-adaptive configurations. Section 6 examines the numerical properties of the two DE methods in detail, using both comparative studies and bulk tests on a very large set (in excess of 250,000) of model and contract parameter configurations. As some of our tests use adaptive Gauss-Lobatto quadrature for benchmarking, we additionally outline how this popular method can be made more performant using the techniques

[3]For those skeptical of any method that is not included in the Numerical Recipes "bible" we are pleased to observe that the Third Edition of NR (see [51]) includes a section dedicated to DE methods. While the code in NR is adequate, we recommend [44] for actual implementation.

[4]Some Finance applications, all unrelated to the problem in this paper, include [7] and [12],

developed in this paper. Section 7 concludes the paper. A series of brief appendices provide some technical details about the methods in the paper, to aid those interested in carrying out actual implementation work.

2 The Heston Model

For simplicity, and without loss of generality, let us assume that the process $F(t)$ is a martingale, such that $F(0) = \mathbb{E}(F(T)) = F_0$. The Heston model of [27] define the dynamics of F as the following 2-dimensional SDE:

$$dF(t) = F(t)\sqrt{v(t)}\,dW(t), \quad F(0) = F_0, \tag{6}$$

$$dv(t) = \kappa(\theta - v(t))\,dt + \epsilon\sqrt{v(t)}dW_v(t), \quad v(0) = v_0, \tag{7}$$

where $\kappa, \theta, \epsilon, v_0, F_0$ are positive constants, and $W(t)$ and $W_v(t)$ are Brownian motions with correlation $\rho \in (-1, 1)$. Taking the limit $\kappa, \epsilon \downarrow 0$ produces the Black-Scholes model $dF(t) = F(t)\sqrt{v_0}\,dW(t)$ as a special case.

There are multiple ways to state the characteristic function ϕ_H of $X(T) = \ln(F(T)/F_0)$ for (6)-(7). To avoid problems with branch-cuts of the complex logarithm, we use the formulation recommended[5] in [1] (see also [40]):

$$\phi_H(u) = e^{A(u) + v_0 B(u)} \tag{8}$$

where

$$A(u) = \frac{\kappa\theta}{\epsilon^2}\left((\beta - D)T - 2\ln\left(\frac{1 - Ge^{-DT}}{1 - G}\right)\right),$$

$$B(u) = \frac{\beta - D}{\epsilon^2}\left(\frac{1 - e^{-DT}}{1 - Ge^{-DT}}\right),$$

and

$$\beta = \kappa - i\epsilon\rho u, \quad G = \frac{\beta - D}{\beta + D}, \quad D = \sqrt{\beta^2 + \epsilon^2 u(u + i)}. \tag{9}$$

We note that the Black-Scholes limit $\kappa, \epsilon \downarrow 0$ results in the characteristic function

$$\phi_{BS}(u) = \exp\left(-\frac{1}{2}v_0 T u(i + u)\right).$$

The Black-Scholes characteristic function $\phi_{BS}(u)$ is analytical in the entire complex plane, but if we extend $\phi_H(u)$ in (8) to complex-valued u, we find that $\phi_H(u)$ has essential singularities at those u for which the transcendental equation

$$G = e^{DT} \tag{10}$$

[5] As written literally below, the formulas for the function ϕ_H are subject to cancellation errors. Appendix A shows how to arrange the calculations to avoid this.

is satisfied. Unfortunately, there is no closed-form solution for (10), so the location of the infinite (but countable) set of singularities must be done numerically (see Section 3.2 and Appendix B). Nevertheless, [41] has shown that all singularities are located on the purely imaginary axis; it is also known (see [36]) that all singularities must lie strictly outside the interval $[-i, 0]$ on the imaginary axis. For later use, let us use $-ik_{\max}$ to denote the singularity closest to $-i$ from the left (i.e., satisfying $k_{\max} > 1$); and let us use $-ik_{\min}$ to denote the singularity closest to 0 from the right (i.e., satisfying $k_{\min} < 0$). Figure 1 shows a typical graph of $|\phi_H|$, with $k_{\max}$ and $k_{\min}$ highlighted.

Figure 1: $|\phi_H(u)|$ for Complex u

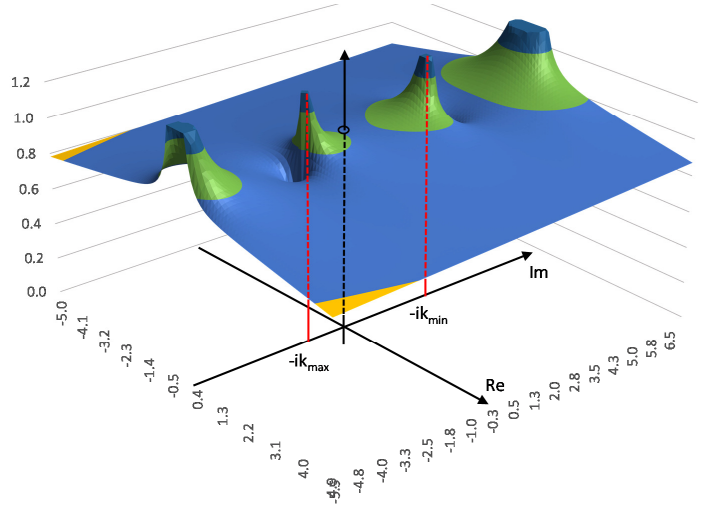

The modulus of the Heston model characteristic function, $|\phi_H(u)|$, as computed from (8). The real ("Re") and imaginary ("Im") values of the argument u are as shown on the axes in the figure. The figure also shows the bound parameters $k_{\min}$ and $k_{\max}$, as given by the location of the nearest singularities (necessarily truncated in the graph) straddling the interval $[-i, 0]$ on the imaginary axis. The model and option parameters were: $F_0 = 110$, $K = 100$, $v_0 = 6.25\%$, $\kappa = 50\%$, $\epsilon = 200\%$, $\rho = 0.2$, and $T = 0.75$.

2.1 Notes on Domain

It is sometimes stated that $\phi_H(u)$ is analytical only in a "strip" or "tube" of the type $u = x - iy$, with y limited to the (real-valued) interval $(k_{\min}, k_{\max})$. This is obviously not accurate[6], since, as just stated, ϕ_H is analytical everywhere save for a countable set of discrete points on the imaginary axis. Nevertheless, ϕ_H is certainly not well-behaved everywhere, especially close to the imaginary axis, and can possibly fail to decay for large arguments. To demonstrate the latter, consider ϕ_H's asymptotic behavior along

[6]For u outside of the strip, the function $\phi_H(u)$ may, however, cease to equal $\mathbb{E}(e^{iuX(T)})$. See [41].

the line $l(x) = \gamma + c \cdot x$, with γ some real constant, x real, and $c = a + ib$ being a complex number with positive real part. We get:

Lemma 1 *Assuming $\kappa, \theta, \epsilon, v_0, F_0, a > 0$, then, for $x \in \mathbb{R}$,*

$$\phi_H(\gamma + (a + ib) \cdot x) \sim \exp\left(\frac{v_0 + \kappa\theta T}{\epsilon} ax\,(q + iw)\right), \quad x \to \infty, \tag{11}$$

with

$$q = \rho\frac{b}{a} - \sqrt{1 - \rho^2}, \quad w = -\rho - \frac{b}{a}\sqrt{1 - \rho^2}. \tag{12}$$

Consequently,

$$\lim_{x\to\infty} |\phi_H((a + ib)x)| = \begin{cases} \infty, & q > 0 \\ 0, & q < 0. \end{cases} \tag{13}$$

The angle φ to the real axis formed by the line $l(x) = \gamma + c \cdot x$ is given by $\tan(\varphi) = b/a$. As such, we note that the decay condition $q < 0$ in Lemma 1 translates into

$$\rho \tan(\varphi) < \sqrt{1 - \rho^2}. \tag{14}$$

If $\rho = 0$, for instance, we just need $\varphi \in (-\pi/2, \pi/2)$ for the characteristic function to decay at a rate of $e^{-const \cdot x}$. For large positive correlations, the decay condition is $\varphi \in (-\pi/2, 0)$; for large negative correlations, it is $\varphi \in (0, \pi/2)$.

For comparison, we note that the Black-Scholes model has asymptote

$$\lim_{x\to\infty} \phi_{BS}((a + ib)x) \approx \exp\left(-\frac{1}{2}v_0 T\left\{x^2(a^2 - b^2) + 2i \cdot s^2 ab\right\}\right)$$

such that $|\phi_{BS}|$ decays to zero at the much faster rate $e^{-const \cdot x^2}$, provided that $\varphi \in (-\pi/4, \pi/4)$ (which implies that $a^2 > b^2$).

3 Angled Contour Shift Integral

Let us focus our attention to the integral

$$I = e^{\alpha\omega} \int_0^\infty \mathrm{Re}\left\{e^{ix\omega} Q_H(x - i\alpha)\right\}\, dx, \quad Q_H(z) = \frac{\phi_H(z - i)}{z(z - i)}, \tag{15}$$

which, from (3), is related to $C(F_0, K)$ through

$$C(F_0, K) = R(\alpha, F_0, K) - \frac{F_0}{\pi} \cdot I. \tag{16}$$

For (16) to be valid, [32] (and many others) show that we must restrict α to ensure that the argument to ϕ_H at $x = 0$ never ventures outside the interval $(-ik_{\max}, -ik_{\min})$ on the imaginary axis. As discussed earlier, we must therefore require that

$$\alpha \in (\alpha_{\min}, \alpha_{\max}), \tag{17}$$

where we have defined

$$\alpha_{\min} = k_{\min} - 1, \quad \alpha_{\max} = k_{\max} - 1. \tag{18}$$

As noticed in [32] and [37] (and others), the integral in I may be written as the real part of a contour integral in the complex plane,

$$I = \text{Re}\left\{\int_C e^{iz\omega} Q(z)\, dz\right\}, \tag{19}$$

where the contour C runs parallel to the real axis, from $-i\alpha$ to $\infty - i\alpha$, with α restricted as in (17). Contour integrals of this form often benefit from a contour deformation to insert exponential decay, especially if $|\omega|$ is large and if $Q(z)$ decays slowly along C. For instance, consider replacing C with an angled line-contour C^* parameterized as

$$C^* : -i\alpha + x\,(1 + i\tan(\varphi)), \tag{20}$$

with $\varphi \in (-\pi/2, \pi/2)$, and the real-valued line parameter x is running from 0 to ∞. For us to be able to change the integration path from C to C^*, conditions on the angle φ in (20) must be met; we list these in the Proposition below.

Proposition 1 *Let Ω be the set of angles φ for which*

$$\tan(\varphi)\, r < \sqrt{1-\rho^2}, \quad r = \rho - \frac{\epsilon\omega}{v_0 + \kappa\theta T}. \tag{21}$$

If

$$\varphi \in \Omega \cap (-\pi/2, \pi/2), \tag{22}$$

then the integral in (19) may be written as

$$I = \text{Re}\left\{\int_{C^*} e^{iz\omega} Q(z)\, dz\right\}.$$

Proof: The closed triangular integration loop ABC in Figure 2 (assume that vertex A coincides with $-i\alpha$) contains no singularities, so, per Cauchy's Residue Theorem, the integral around the loop will equal zero. Consider now moving vertex B towards infinity, while retaining the right-angled triangular loop. For integrals along segments AB and AC to be equal in the limit, a sufficient condition is that the integrand along the line-segment BC will approach zero sufficiently fast, say, exponentially. If we define the complex-valued function

$$h(x) = -i\alpha + x\,(1 + i\tan(\psi)) \tag{23}$$

a sufficient condition is that, for every value of the real-valued angle ψ between 0 and φ (see Figure 2),

$$\lim_{x\to\infty} \left| e^{ih(x)\omega} Q(h(x)) \right| = 0,$$

with the decay to zero being exponentially fast. As the denominator of Q decays quadratically in x, it suffices to examine the quantity $e^{ih(x)\omega}\phi_H\left(h(x)-i\right)$. It also suffices to examine the case $\psi=\varphi$. Now,

$$\left|e^{i(x(1+i\tan(\varphi)))\omega}\phi_H\left(x\left(1+i\tan(\varphi)\right)\right)\right| = \left|e^{-x\tan(\varphi)\omega}\phi_H\left(x\left(1+i\tan(\varphi)\right)\right)\right|.$$

From Lemma 1, we see that the right-hand side will decay exponentially to zero for large x, provided that

$$-\tan\left(\varphi\right)\omega+\frac{v_0+\kappa\theta T}{\epsilon}q<0,$$

where $q=\rho\tan(\varphi)-\sqrt{1-\rho^2}$, per (12). In other words, we require

$$\tan(\varphi)\left(\rho\frac{v_0+\kappa\theta T}{\epsilon}-\omega\right)<\frac{v_0+\kappa\theta T}{\epsilon}\sqrt{1-\rho^2}.$$

If φ is so restricted, exponential decay is easily seen to be assured for all angles ψ between 0 and φ. This proves the Proposition. ∎

Figure 2: Integration Loop Schematic

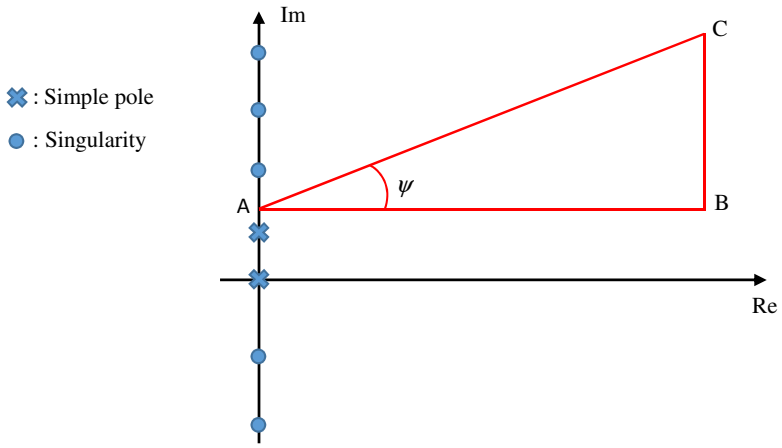

A closed integration loop in the complex plane. Poles and singularities of the integrand in (15) are all located on the imaginary axis, as indicated.

Proposition 1 allows us to recast the original integral in (15) as

$$\begin{aligned} I &= \text{Re}\left\{\int_0^\infty e^{ih(x)\omega}Q(h(x))\ \left(1+i\tan(\varphi)\right)dx\right\} \\ &= e^{\alpha\omega}\int_0^\infty \text{Re}\left\{e^{-x\tan(\varphi)\omega}e^{ix\omega}Q(h(x))\ \left(1+i\tan(\varphi)\right)\right\}\ dx, \end{aligned} \tag{24}$$

with $h(x)$ given in (23). Notice how we have managed to insert an exponential factor $e^{-x\tan(\varphi)\omega}$ into the integral, which, if $\tan(\varphi)\omega$ is positive, can dampen out oscillations in the integrand. Notice also that the speed of decay is proportional to ω, a fortunate circumstance given that the Fourier oscillator $e^{ix\omega}$ is mostly problematic when ω is large.

3.1 Selection of φ

In (24), one may be tempted to pick extreme values of φ (subject to the bound (22), of course) to make the decay of the integrand as high as possible. However, this will likely move the integration contour C^* dangerously close to the singularities of ϕ_H, so in practice one needs to establish a reasonable rule for picking φ. We establish one such rule here.

Let r be as in Proposition 1, i.e.,

$$r = \rho - \frac{\epsilon\omega}{v_0 + \kappa\theta T}.$$

Then, we use the heuristic

$$\varphi = \begin{cases} \frac{\pi}{12} \cdot \operatorname{sgn}(\omega), & r\omega < 0, \\ 0, & r\omega \geq 0. \end{cases} \tag{25}$$

To explain the rationale for (25), we note that there are two main sources of problematic behavior of the integrand: one is the exponential factor $e^{-x\tan(\varphi)\omega}$, when $\tan(\varphi)\omega$ is negative; the other is correlation as filtered through r. Each of these sources causes bad behavior only on one side of the real axis. When both introduce problems on the same side, as indicated by the condition $r\omega < 0$, it is clear that the contour should point away from the "bad" side, which explains the $\operatorname{sgn}(\omega)$ term. The value $\pi/12$ was determined by performance tuning the method using bulk testing[7]. When both sources introduce bad behavior on opposite sides of the real axis, then whichever direction we go in, we will be moving towards poor numerical behavior. Taking $\varphi = 0$ steers clear of trouble, and in practice we found that this works as well as other, more complicated, choices.

3.2 Selection of α

We use the *optimal* α method of [39] and fill in some details. First, notice that taking $\alpha \in (-1, 0)$ will result in cancellation errors. This is clear since in this case the option value formula has the form $C = F_0 - I$ for a call and $P = K - I$ for a put, where the integral term I must be positive. The computed option price, if non-zero, cannot be smaller than the residue term (F_0 or K) times the machine epsilon ε. Even if the integral term were computed to full machine precision, the maximum digits of accuracy achievable for a

[7] $\pi/12$ may appear quite conservative relative to the theoretical cutoff of $\pi/2$, but we should keep in mind that Proposition 1 only tells us about the asymptotic behavior of the integrand along the chosen contour C^*, and does not rule out poor numerical behavior when the angle of the contour is too close to the cutoff.

call is $\log_{10}(1/\varepsilon) + \log_{10}(C/F_0)$ (and similarly for a put where P/K replaces C/F_0). That is, if C/F_0 is on the order of 10^{-d}, then we must lose d digits of accuracy.

To avoid cancellation, for both puts and calls we choose $\alpha < -1$ when $\omega > 0$, and $\alpha > 0$ when $\omega < 0$. This policy ensures that the residue term is always equal to the option intrinsic and therefore $-I$ is always equal to the time value of the option. Since both terms are then positive, no cancellation can take place. In summary, we will therefore require, as a minimum, that $\alpha \in (\alpha_{\min} - 1) \cup (0, \alpha_{\max})$.

To sharpen our choice of α further, we follow [39] and select

$$\alpha^* = \operatorname{argmin} \{\ln \phi_H(-(\alpha+1)i) - \ln(\alpha(\alpha+1)) + \alpha\omega\}, \tag{26}$$

where the minimum is taken over $(\alpha_{\min}, -1)$ or $(0, \alpha_{\max})$ as appropriate. The procedure for choosing α consists of three steps:

1. For $\omega \geq 0$ take $\alpha < -1$; for $\omega < 0$ take $\alpha > 0$.
2. For $\alpha < -1$, locate $\alpha_{\min}$; for $\alpha > 0$, locate $\alpha_{\max}$.
3. Set $\alpha = \alpha^*$, where α^* solves the minimization problem (26).

Given a search interval $(\alpha_{\min}, -1)$ or $(0, \alpha_{\max})$, the solution of (26) in Step 3 is straightforward (the objective function is concave), and can be done with a one-dimensional algorithm such as *Brent's method* (see [51], for instance). The location of $\alpha_{\min}$ and $\alpha_{\max}$ in Step 2 is essentially a root-search problem, easily solved numerically if we can bracket the roots. As the root bracketing exercise has a few moderate complications, we discuss it in Appendix B, leaning on work by [4] and [52].

3.3 A Quick Numerical Example

In Figure 3 below, we use an in-the-money option to confirm that our recommendation for α and φ improve the numerical properties of the integrand in (24). As we can see from the two graphs in the figure, the oscillations in the tail of the integrand are dampened considerably with the recommended parameter setting. Not directly obvious from the figure is of course also that fact that our recommended choice of α is such that cancellation errors in the option price formula are remedied.

4 The DE-C Double-Exponential Quadrature Rule

So far, we have demonstrated how the key integral in the Heston model option computation can be restated as (24), and have provided guidance as to how to select the two free parameters α and φ to make (24) amenable to evaluation by a numerical quadrature scheme. These results are essentially generic and would likely benefit any quadrature rule (see Section 6.2 for an example of this, using Gauss-Lobatto quadrature). For reasons already touched upon, our specific choice of quadrature scheme is here the double-exponential (DE) rule, which we present below. For later ease of reference, the application of a basic DE scheme to the angled contour integral in (24) is denoted the *DE-C method*.

Figure 3: Integrand in (24) for different φ and α

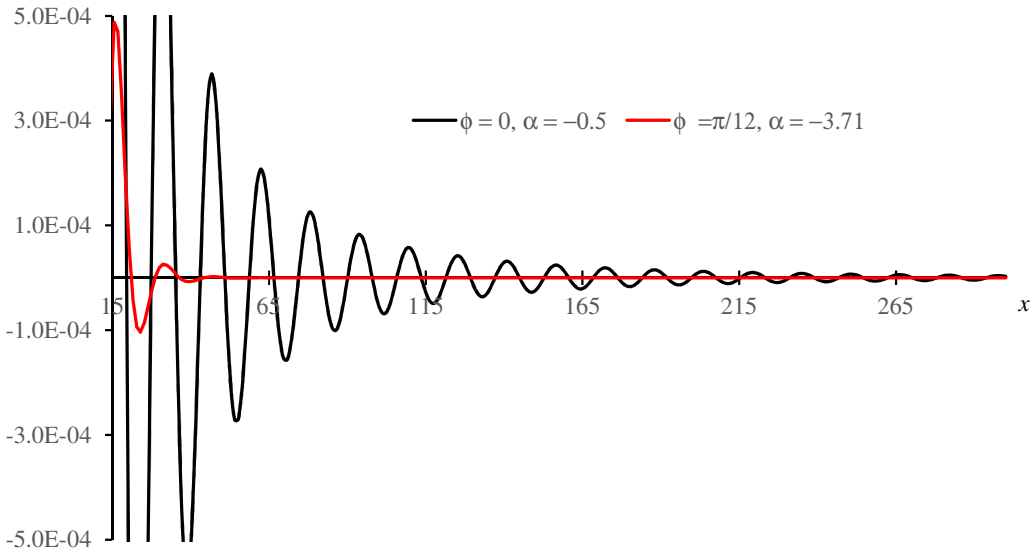

The graph shows the tail of the integrand in (24) as a function of the integration variable x, with $x \geq 15$. One graph uses the current industry-standard settings of $\varphi = 0$ and $\alpha = -1/2$; another graph uses the recommendations in Sections 3.1 and 3.2 to set $\varphi = \pi/12$ and $\alpha = -3.71$. The model and option parameters were: $F_0 = 150$, $K = 100$, $v_0 = \theta = 1\%$, $\kappa = 10\%$, $\epsilon = 200\%$, $\rho = 0.8$, and $T = 1.0$.

4.1 DE fundamentals

DE quadrature is motivated by the fact that the trapezoid rule is very efficient for integrals over $\mathbb{R}$ of functions that are analytic in a strip containing the real axis; see [62] for an overview. When the integrand decays double-exponentially, the trapezoid rule is quadratically convergent in a spectral sense, with halving the step-size roughly doubling the number of correct digits. In fact, Sugihara [59] has shown that, in a formal sense, the trapezoid rule is optimal for such integrals.

Keeping the result of [59] in mind, suppose now we are given an integral

$$I = \int_a^b f(x)\,dx$$

where f is analytic on (a, b); either endpoint may be finite or infinite. The idea is to apply a transformation $x = g(t)$,

$$g'(t) > 0, \quad g(-\infty) = a, \quad g(+\infty) = b,$$

so that

$$I = \int_{-\infty}^{\infty} g'(t) f(g(t))\,dt$$

and the transformed integrand decays double-exponentially as $t \to \pm\infty$, in the sense that $|g'(t)f(g(t))| = O(\exp(-c\exp(|t|)))$ for large $|t|$. Then the trapezoid rule is applied with step-size h to arrive at the approximation

$$I_h = h\sum_{n=-\infty}^{\infty} g'(nh)f(g(nh)) = h\sum_{n=-\infty}^{\infty} w_n f(x_n), \tag{27}$$

where $w_n = g'(nh)$ are weights and $x_n = g(nh)$ are the abscissas of the quadrature rule.

For a given step-size h, (27) in practice needs to be truncated at a finite number of terms. Rather than crudely using a constant limit N for the number of terms in the upper and lower sums, we instead will always stop the sums when contributions from new terms are insignificant, as defined by a threshold. A basic implementation for a fixed h would then look like this:

1. For $n = -1, -2, \ldots$, add up terms $w_n f(x_n)$ until, say, two consecutive terms fall below some threshold. Call this sum S_l.
2. For $n = 0, 1, \ldots$, add up terms $w_n f(x_n)$ until two consecutive terms fall below the threshold. Call this sum S_u.
3. Then $I \approx h(S_l + S_u)$.

If we take the threshold in Steps 1 and 2 to be the machine epsilon ε times the current partial sum, then the issue of truncation error is side-stepped. As the terms drop off rapidly this is an economical procedure, though other heuristics may be more efficient.[8]

4.2 Automatic Exp-Sinh Rule

Since the integrals we are dealing with are of the semi-infinite form

$$I = \int_0^{\infty} f(x)\,dx \tag{28}$$

it is natural to use the *exp-sinh* transformation from [60]:

$$x = g(t) = \exp\left(\frac{\pi}{2}\sinh t\right),$$

which gives

$$x_n = \exp\left(\frac{\pi}{2}\sinh(nh)\right),$$
$$w_n = \frac{\pi}{2}\cosh(nh)\exp\left(\frac{\pi}{2}\sinh(nh)\right),$$

[8] For instance, [45] recommend using ε as the threshold. We use this criterion in our tanh-sinh implementation.

to be applied in the trapezoid formula (27).

The resulting integration method has several advantages over the quadrature rules usually proposed in the Heston literature. First, as mentioned above, it finesses the issue of truncation error. Second, compared with transformation to a finite interval, the exp-sinh method avoids the problem of selecting an effective quadrature scheme for the transformed integral: we already know from [59] that the trapezoid rule is optimal in this case. Third, the simplicity of the trapezoid rule leads to a compact implementation of an automatic scheme (See [44] and [64] for details).

For our purposes here, we use a simple automatic exp-sinh scheme as our reference method. Here, at each stage the step-size h is halved and the procedure terminates when two successive estimates differ by less than a requested relative error. To determine the initial step-size h, it is convenient to choose N, where[9] $2N + 1$ is a proxy for the number of nodes used at the first level, and choose h from

$$Nh = 4.25, \tag{29}$$

a relationship that was estimated by trial and error. For our later numerical tests, we used $N = 10$, and also imposed a limit of eight levels of subsequent refinement.

4.3 Fixed Tanh-Sinh Rule

As a simpler alternative to the automatic exp-sinh rule above, we can use a *fixed* double-exponential quadrature scheme. Here, we just want to prescribe a fixed step size and get back an accurate result, and we can live without an error estimate. For this, we use the *tanh-sinh* rule which is based on the transformation

$$x = \tanh\left(\frac{\pi}{2}\sinh t\right) \tag{30}$$

which maps $(-1, 1)$ to $(-\infty, +\infty)$. We choose this rule over the exp-sinh rule above, in part because we, as shown below, may use a well-performing heuristic from [62] to set the step size. Additionally, using tanh-sinh adds some variety in our test of double-exponential mappings, and also allows us to discuss the issue of how best to map the semi-infinite range of our integrals on to a finite one.

As a first step in the application of the tanh-sinh rule, we need to find a mapping function u that translates the integral in (28) into an integral on $(-1, 1)$, i.e.,

$$I = \int_0^\infty f(z)\,dz = \int_{-1}^1 u(x)\,dx.$$

In the Heston literature, the mapping of $(0, \infty)$ on to a finite domain is often done through the relationship mapping $z = -const \cdot \ln(x)$ (see, e.g., [39]), where the constant is determined by the asymptotics of the characteristic function. While this mapping has compelling theoretical properties, numerical tests on a variety of quadrature rules strongly

[9] $2N + 1$ since the trapezoidal sum in (27) is proxied as running from $-N$ to N.

favored the simpler transformation

$$z = (1+x)/(1-x). \tag{31}$$

Using this mapping, we get

$$\int_0^\infty f(z)\,dz = \int_{-1}^1 u(x)\,dx, \quad u(x) \triangleq \frac{2}{(1-x)^2} f\left(\frac{1+x}{1-x}\right). \tag{32}$$

Given a step-size h, an application of the DE tanh-sinh transformation to the intermediate function (32) yields, from (27), the quadrature rule

$$I_h = h \sum_{n=-\infty}^{\infty} w_n u(x_n), \tag{33}$$

where

$$x_n = \tanh\left(\frac{\pi}{2}\sinh(nh)\right),$$
$$w_n = \frac{\frac{\pi}{2}\cosh(nh)}{\cosh^2\left(\frac{\pi}{2}\sinh(nh)\right)}.$$

In practice, it is better numerically to generate

$$q_n = \exp(-\pi\sinh(nh)), \quad y_n = 1 - x_n = \frac{2q_n}{1+q_n}, \quad w_n = \frac{1}{1+q_n} y_n \pi \cosh(nh).$$

To determine h, we again choose N, where $2N+1$ is a proxy for the number of nodes used in the trapezoidal sum (33). As an improvement over (29), for the tanh-sinh method, we use a heuristic for the optimal step-size suggested by [62]:

$$h = \frac{W(2\pi N)}{N},$$

where W is the Lambert W-function, defined implicitly by $z = W(z)\exp W(z)$. See [63] for a simple, fast method to compute W to near double precision accuracy. As was the case earlier, we do not literally use N as a way to terminate the summations in (33), but instead use the threshold termination criterion outlined in Section 4.1. The actual number of integrand evaluations will therefore in practice differ from $2N+1$.

5 The DE-O Double-Exponential Quadrature Rule

A key "trick" in the DE-C method was the dampening of oscillations in the integrand through a shift of the integration contour in the complex plane. Another strategy is to allow for an oscillatory integrand, but adapt the node placement of the quadrature scheme to account for the oscillations. The *DE-O method* outlined in this section couples this idea with double-exponential integration, addressing simultaneously the problems of oscillation and slow decay in the integrand. We base the approach on a Fourier integral technique developed by [48] and [49]. A further refinement was later given by [50], and is the version we use.

5.1 Ooura's Method for Fourier Transforms

For our uses, we focus on Approximation Formula 2 from[10] [50], noting that this is an improvement over [49] which requires splitting the integral into separate sine and cosine integrals with different quadrature points, effectively doubling the number of function evaluations. To present the relevant formula, consider

$$J(\omega) = \int_0^\infty f(x)e^{i\omega x}\,dx, \quad \omega > 0,$$

where f may be complex-valued.[11] The idea is to choose a mapping, $x = Mg(t)$, where $M > 0$ is a constant, $g'(t) > 0, g(-\infty) = 0, g(+\infty) = \infty$, such that

$$\begin{aligned} &\text{as } t \to -\infty, \quad g'(t) \to 0, \text{ double-exponentially, and} \\ &\text{as } t \to +\infty, \quad g(t) \to t, \text{ double-exponentially.} \end{aligned}$$

The transformed integral is then

$$J(\omega) = M\int_{-\infty}^{+\infty} f(Mg(t))g'(t)e^{i\omega Mg(t)}\,dt.$$

Define

$$E(\omega) = M\int_{-\infty}^{+\infty} f(Mg(t))g'(t)e^{i\omega Mt}\,dt.$$

Then, the key point is that, per [50], $|E(\omega)|$ decays exponentially to zero as M becomes large. Hence, we can calculate $\tilde{J}(\omega) = J(\omega) - E(\omega)$ in place of $J(\omega)$, with $E(\omega)$ effectively serving as a control variate. Using

$$e^{i\omega Mg(t)} - e^{i\omega Mt} = \left[e^{\frac{1}{2}i\omega M(g(t)-t)} - e^{-\frac{1}{2}i\omega M(g(t)-t)}\right] e^{\frac{1}{2}i\omega M(g(t)+t)}$$

we get

$$\tilde{J}(\omega) = 2iM\int_{-\infty}^{+\infty} f(Mg(t))g'(t)\sin\left(\frac{1}{2}\omega M(g(t)-t)\right)\exp\left(\frac{i}{2}\omega M(g(t)+t)\right)\,dt.$$

It can easily be seen that the integrand here decays double-exponentially as $t \to \pm\infty$, so we expect the trapezoid rule to be effective. For our purposes it is sufficient to take

$$h = \pi/(M\omega), \tag{34}$$

yielding the trapezoidal approximation

$$J(\omega) \approx \tilde{J}_h(\omega) \triangleq \frac{2i\pi}{\omega}\sum_{n=-\infty}^{+\infty} f\left(\frac{\pi}{h\omega}g(nh)\right)g'(nh)\sin\left(\frac{\pi}{2h}(g(nh)-nh)\right)\exp\left(\frac{i\pi}{2h}(g(nh)+nh)\right). \tag{35}$$

[10] We are only interested in the case $\omega = \omega_0$.

[11] For $\omega < 0$ we can simply use conjugation: $J(\omega) = \overline{J(-\omega)}$.

Following [49] and [50], the concrete transformation we use is given by

$$g(t) = \frac{t}{1 - \exp(-2t - A(1 - e^{-t}) - B(e^t - 1))},$$

with[12]

$$B = .25, \quad A = .66 \times \frac{B}{\sqrt{1 + M \ln(1 + M)/(4\pi)}}.$$

Note that for the transformation to be robust, it is crucial that A (and therefore g) to depend on M in this manner. For $t = 0$, we use

$$g(0) = \lim_{t \to 0} g(t) = \frac{1}{2 + A + B},$$
$$g'(0) = \lim_{t \to 0} g'(t) = \frac{1}{2}\left(1 + \frac{A - B}{(2 + A + B)^2}\right).$$

The first limit is trivial; the second requires a bit of care with the algebra.

The choice of h (and, through (34), the choice of M) is described in [49], and our implementation in this paper uses the automatic, threshold-based procedure in that paper. We note that the scheme is not *progressive*. That is, as we refine the mesh, we cannot reuse the previous function evaluations. This seems unavoidable given that the quadrature nodes are $Mg(nh)$, and M varies with h in (34). On the other hand, this frees us from having to halve the step-size at each level of the automatic procedure; instead, we can regain some efficiency by choosing the next step-size according to the current error estimate. [49] contains the details, with Appendix C offering some details on how to best implement the terms of the trapezoidal sum (35).

5.2 Additional Details for Heston Case

For the specific application of Ooura's method the Heston model integral in (24), we need a strategy for setting φ and α. For the former, we recall that the purpose of a non-zero value of φ is to dampen oscillations in the integrand. As the DE-O model is fundamentally designed to embrace oscillations, we elect to simply set $\varphi = 0$. For additional simplicity[13], we also set $\alpha = -1/2$, thereby avoiding the complications of searching for an optimal α. In addition, with the choice $\alpha = -1/2$ all calculations for the important case $\rho = 0$ reduce to real arithmetic, yielding a nice performance boost and also simplifying the implementation. As the DE-O method does not control the residue term in (4), it is subject to the cancellation problem discussed in Section 3.2, although that often does not matter much in practice. E.g., in double precision arithmetic we can still calculate the value of a call option worth on the order of $F \cdot 10^{-8}$ to about 8 digits.

Finally, it should be noted that the technique in [50] does not apply when the Fourier term produces no oscillations (i.e., when options are at-the-money and therefore $\omega = 0$).

[12] Here we have added the ad-hoc factor .66 to the expression for A. This resulted in somewhat improved performance in our bulk timing tests.

[13] This can be relaxed, of course.

For this case, we simply switch to use the automatic exp-sinh method (with $\alpha = -1/2$ and $\varphi = 0$) outlined earlier.

6 Numerical Results

For our tests, we organize our results into four broad sections. First, we describe an adaptive Gauss-Lobatto quadrature method for benchmarking purposes, and use this method in a bulk test setting for independent validation of the efficacy of the angled contour method of Section 3. Second, we conduct a small warm-up exercise where we test double-exponential tanh-sinh and exp-sinh quadrature on set of testing configurations defined in [39]. Third, we run a full-blown bulk test of the DE-C method, against several alternative schemes. Finally, we test the DE-O method.

With the exception of the tests based on [39], all our numerical experiments are of the bulk type[14], referencing a large set of model and contract parameters that aim to exhaustively cover the space of parameters that might be encountered in real applications. We list the details of the test in Section 6.1 below, and note that many of the cases are substantially more challenging than what can be found in the existing literature. In particular, we highlight that the tests cover the problem cases of very[15] short maturities as well as moneyness settings that are very far from at-the-money. Additionally, we cover a wide range of model parameters, both in correlation, vol-of-vol, and volatility spaces.

6.1 Bulk Test Configuration

For our bulk test, we consider European put option pricing with a variety of model and contract parameters. In one set of tests we freeze the strike to $K = 100$, and let the initial forward vary as $F_0 \in \{100, 100.0001, 101, 110, 200, 10^3, 10^4\}$; in another, we freeze the forward at $F_0 = 100$, and let the strike vary as $K \in \{100.0001, 101, 110, 200, 10^3, 10^4\}$. These choices of F_0 and K ensure that we test put options at all levels of moneyness, ranging from deeply in-the-money to deeply out-of-the-money. For each of the resulting 13 combinations of F_0 and K, we then vary the remaining model and contract parameters

[14] Tests on small sets of parameters are, in our opinion, mostly unconvincing, given the how the challenges of the integrand vary strongly across different model and contract parameters. Examples of this will become evident shortly. For instance, the non-angled adaptive GL method performs reasonably well on the small set of tests in [39], yet displays substantial lack of robustness in our more challenging bulk tests.

[15] We have values of T as low as 0.0025 years, or less than a single day. While options are rarely traded with such short maturities, the passage of time will, of course, guarantee that even long-dated options will eventually have less than one day left before they mature.

as follows:

$$\begin{aligned} T &\in \{0.0025, 0.1, 0.5, 2, 10, 30\}\,; \\ v_0 &\in \{0.0001, 0.0025, 0.04, 0.25, 1\}\,; \\ \theta &\in \{0.0001, 0.0025, 0.04, 0.25, 1\}\,; \\ \kappa &\in \{0.01, 0.1, 0.5, 2\}\,; \\ \epsilon &\in \{0.0001, 0.1, 0.5, 1, 3\}\,; \\ \rho &\in \{-0.95, -0.5, -0.1, 0, 0.1, 0.5, 0.95\}\,. \end{aligned}$$

In total, our bulk test therefore covers 273,000 separate model and contract configurations.

6.2 Benchmark: Improved Gauss-Lobatto Quadrature

For our comparative tests, we need a reference method that can reliably compute the integrals to good accuracy and which is simple to implement. A natural starting point is the adaptive Gauss-Lobatto (GL) method presented in [24], a method that has been used as a benchmark elsewhere in the Heston literature (e.g., [33], [39], [40], [55]). As [24] gives full details, along with Matlab code, we will not go into general implementation details here. We will, however, make a few targeted modifications to the standard implementation, to allow the method to perform with acceptable efficiency on our bulk test. First, for the necessary mapping to a finite closed interval needed for GL quadrature, we use the transform (31), rather than the standard methods suggested in the literature. Second, we want to apply the GL algorithm to the angled contour integral (24), rather than to the basic integral in the literature (i.e., the case where $\varphi = 0$).

As a warm-up test, let us consider how the choice of φ affects the performance of the adaptive GL method when applied to the pricing of put options. Table 1 below shows the results of our bulk tests on two separate quadrature configurations: i) the standard choice of $\varphi = 0$ ("Non-Angled") and ii) the choice of φ in Section 3.1 ("Angled"). For both cases, the parameter α was set to the optimal value discussed in Section 3.2.

As Table 1 shows, for a given requested tolerance the angled GL method not only consumes about 10-20 times less function evaluations than the standard, non-angled GL method, it also achieves a realized tolerance that is up to 4 orders of magnitude better. The table also shows that the non-angled GL method is not robust throughout our challenging bulk test space, as the number of function evaluations sometimes will balloon into several millions, typically when the integrand is short-dated and is far from being at-the-money. In contrast, the angled GL is everywhere able to contain the worst-case computational efforts to reasonable levels. Finally, while realized precision is lower than requested precision for both methods, the angled GL method achieves substantially higher realized precision than non-angled GL.

Table 1: Gauss-Lobatto Bulk Tests

	GL Non-Angled			*GL Angled*		
Tolerance	Avg (Max) FEs	RRMSE	Max Rel Error	Avg (Max) FEs	RRMSE	Max Rel Error
1.E-07	2,838 (1,116,898)	6.2E-02	2.9E+01	312 (2,928)	1.1E-03	5.4E-01
1.E-09	8,244 (3,885,048)	2.4E-03	7.6E-01	595 (5,628)	5.9E-07	1.1E-04
1.E-11	20,599 (9,827,178)	5.6E-05	2.4E-02	1,131 (10,158)	2.4E-09	1.1E-06

Bulk test performance results for put option pricing with Gauss-Lobatto quadrature. Test cases cover the contract and model parameter ranges outlined in Section 6.1. "GL Non-Angled" is adaptive Gauss-Lobatto applied to (24) with $\varphi = 0$; "GL Angled" is adaptive Gauss-Lobatto applied to (24) with φ set as in Section 3.1. The "Tolerance" column is the *requested* relative put price error for the adaptive quadrature rule; whereas the "RRMSE" is the average *realized* relative tolerance, expressed as a root-mean-square average. To compute the empirical RRMSE, we used high-precision option prices from the automatic exp-sinh DE-C method in Section 4, set at a relative tolerance of 10^{-15}. In addition to the RRMSE estimate, we also list the maximum relative error ("Max Rel Error") encountered in the bulk tests. Further gauges of computational efficiency in the table include the average and worst-case number of evaluations of the integrand ("Average FEs" and "Max FEs", respectively).

6.3 Double-Exponential Quadrature applied to Test in [39]

Armed with confidence that the angled contour method is worthwhile, we now conduct another small warm-up test where we examine the performance of DE quadrature on the parameter cases covered in Table 2 of [39]. The authors here recommend using adaptive Gauss-Lobatto quadrature, so we include results for this method for comparative purposes. The test in Table 2 of [39] is one of the relatively few attempts at a bulk experiment in the literature, and covers 2,280 distinct cases by varying contract parameters only (strike and maturity, specifically); the Heston model parameters are kept fixed. The values of T and K are listed in the caption to Table 2 below, and, we note, are far more benign than those of our own bulk test above, with all values of T in excess of 1 year and ω limited to the comparatively narrow range $[-2.3, 1.4]$.

Our results are shown in Table 2, covering both the (classical) case where the contour angle φ is zero, as well as the case where φ is set as in Section 3.1. We test both the automatic (exp-sinh) and the fixed (tanh-sinh) versions of DE quadrature in Section 4. For consistency with the original data, we used adaptive Gauss-Lobatto quadrature with a relative error tolerance of 10^{-15} as the benchmark[16].

To comment on Table 2, we first notice that the results confirm the observation of Table 1 above: using an angled contour significantly improves the efficiency and robustness of all quadrature schemes tested, even for the relatively benign test case in the table. Second, we observe that for a given level of computational effort (as measured by integrand evaluations) the DE quadrature methods are several orders of magnitude more precise, both on average and for the worst-case scenarios. For instance, for angled contour integration with around 300 evaluations of ϕ_H, the exp-sinh and tanh-sinh DE methods are, on average, roughly 5-6 orders of magnitude more precise than the GL

[16]The often poor realized precision documented in Table 1 for GL quadrature with $\varphi = 0$ was far less pronounced on the much more benign parameter space used in [39].

Table 2: Test Case of [39]

		Non-Angled			*Angled*		
Method	Tolerance	Avg FEs	Max IV Error	Avg IV Error	Avg FEs	Max IV Error	Avg IV Error
GL	1.E-15	4,910	Benchmark	Benchmark	3,256	Benchmark	Benchmark
GL	1.E-07	353	5.1E-06	4.8E-09	247	8.4E-08	3.0E-10
GL	1.E-10	955	1.0E-12	2.2E-12	645	4.9E-11	1.4E-13
Auto DE	1.E-07	380	1.8E-09	1.2E-12	194	1.7E-09	1.0E-12
Auto DE	1.E-10	590	3.4E-14	8.8E-17	291	1.2E-12	5.8E-16
Fixed DE	N=200	166	1.2E-03	4.3E-06	164	1.6E-09	1.2E-11
Fixed DE	N=400	296	8.2E-05	1.9E-07	292	2.4E-14	1.6E-16

Performance of the DE method on the test data of Table 2 of [39]. "Non-Angled" fixes $\varphi = 0$ in the integrand (24); "Angled" sets φ as in Section 3.1. In all cases, α is set to the "optimal" level described in Section 3.2. For the DE method, results are listed for both the automatic exp-sinh method ("Auto DE") and the fixed tanh-sinh method ("Fixed DE"). For methods other than fixed DE quadrature, the "Tolerance" column is the *requested* relative tolerance for the adaptive quadrature; for the fixed DE method the "Tolerance" column lists the proxy value N for the range of the trapezoidal sum, as described in Section 4.3. For consistency with [39], reported average ("Avg IV Error") and maximum ("Max IV Error") errors are everywhere measured in implied volatility terms. To compute the realized empirical errors, we used adaptive GL quadrature ("GL") as the benchmark, with a relative tolerance of 10^{-15}, as indicated in the top row of the table. "Avg FEs" denote the average number of evaluation of the integrand across the test cases. The Heston model parameters were: $F_0 = 1, v_0 = \theta = 0.16, \kappa = 1, \epsilon = 2, \rho = -0.8$. The options priced were call options, with contract parameters picked from the following sets: $K \in \{1/10, 2/10, \ldots, 4\}$, $T = \{1, 5/4, 6/4, \ldots, 15\}$.

method, respectively. Of course, a fair comparison against the existing literature would compare non-angled GL against angled DE (i.e., the DE-C method), in which case the performance (and robustness) gains of our DE methods are even more significant.

6.4 DE-C Bulk Test

With the warm-up tests under our belt, we dispense with all methods that set $\varphi = 0$, as these are evidently not competitive. In Table 3, we compare performance of the automatic and non-automatic DE-C method to adaptive GL, using the bulk test configuration of Section 6.1. Besides adaptive GL, we also implemented a variety of other classic quadrature methods, the results of some of which are shown in the table as well. In the table, we used the automatic exp-sinh scheme with a tolerance of 10^{-15} as the high-precision benchmark used for empirical error computation. We were not able to use the adaptive GL for this, as the convergence patterns for this method revealed that the best achievable relative accuracy of the adaptive Gauss-Lobatto method was about 10^{-12}. In contrast, neither flavor of the DE-C method had this limitation.

It is clear that both flavors of the DE-C scheme are many orders of magnitude more efficient than (angled) GL quadrature. For instance, for about 4-500 integrand evaluations, adaptive GL quadrature produces an average relative precision of around 10^{-6}, whereas the automatic DE-C method has errors in the range of 10^{-12}, i.e. 6 orders of magnitude

Table 3: Bulk Test of DE-C and other Methods

Method	Tolerance	Avg (Max) FEs	RRMSE	Max Rel Error	Options/Sec
Auto DE-C	1.00E-15	806 (4,145)	Benchmark	Benchmark	3,769
Fixed DE-C	N=200	151 (276)	1.1E-04	1.0E-02	18,437
Fixed DE-C	N=400	269 (495)	2.9E-07	3.5E-05	10,721
Fixed DE-C	N=600	380 (700)	2.2E-09	2.7E-07	7,770
Fixed DE-C	N=800	486 (897)	1.6E-11	2.2E-09	6,141
Fixed DE-C	N=1,000	589 (1,090)	4.7E-13	7.4E-11	5,093
Auto DE-C	1.E-04	151 (3,731)	2.7E-05	5.0E-03	18,310
Auto DE-C	1.E-06	235 (3,833)	3.1E-07	1.4E-04	12,206
Auto DE-C	1.E-08	328 (3,880)	6.2E-10	1.8E-07	8,957
Auto DE-C	1.E-10	426 (3,892)	1.2E-13	2.1E-11	6,991
Auto DE-C	1.E-12	524 (4,145)	3.9E-14	4.9E-12	5,706
GL	1.E-05	167 (1,548)	3.9E-03	5.5E-01	19,356
GL	1.E-06	227 (2,148)	1.4E-03	5.4E-01	14,730
GL	1.E-07	312 (2,928)	1.1E-03	5.4E-01	10,985
GL	1.E-08	429 (3,618)	1.6E-06	2.7E-04	8,129
GL	1.E-09	595 (5,628)	5.9E-07	1.1E-04	5,944
GL	1.E-11	1,131 (10,158)	2.4E-09	1.1E-06	3,184
GL	1.E-13	2,192 (28,098)	1.8E-11	2.7E-09	1,663
Clenshaw-Curtis	N=1,000	909 (1,000)	1.4E-04	9.0E-03	4,085
Clenshaw-Curtis	N=1,500	1,364 (1,500)	5.8E-06	4.0E-03	2,758
Gauss-Legendre	N=1,000	910 (1,000)	1.2E-04	6.7E-03	4,030
Gauss-Legendre	N=1,500	1,365 (1,501)	5.1E-05	3.8E-03	2,734

Bulk test performance results for put option pricing with a range of quadrature schemes. For all cases we use the integrand (24) with φ set as in Section 3.1. Test cases cover the contract and model parameter ranges outlined in Section 6.1. "GL" is adaptive Gauss-Lobatto; "Auto DE-C" is the exp-sinh flavor of the DE-C scheme from Section 4.2; "Fix DE-C" is the tanh-sinh flavor of the DE-C scheme from Section 4.3. For the GL and Auto DE-C methods, the "Tolerance" column is the *requested* relative tolerance for the adaptive quadrature; for all other methods "Tolerance" column lists the proxy value N for the range of the quadrature summation (as described in Section 4.3 for the Fix DE-C method, for instance). Other columns are as in Table 1, with the addition a speed metric capturing the average number of option evaluations per second ("Options/Sec"). Tests were performed using a C++ implementation, built with Visual Studio, running single-threaded on a single 2.66 GHz Intel processor. No caching (e.g., as in [31]) was deployed in the tests.

smaller[17]. The classical Clenshaw-Curtis and Gauss-Legendre quadratures included in the table were not competitive, and performed overall worse than the Gauss-Lobatto scheme. We note that the automatic DE-C scheme was overall a bit more efficient than the fixed DE-C rule; but the fixed rule has the virtue of limiting the number of function evaluations in difficult cases.

[17]Of course, a fair comparison to the literature would again use the non-angled GL method, in which case our ED-C method is more than 10 orders of magnitude more precise

6.5 DE-O Bulk Test

As the DE-O method is exposed to the cancellation problem discussed in Section 3.2, using relative errors in bulk tests will produce essentially meaningless results. We consequently use absolute errors instead. The results are given in Table 4.

Table 4: Bulk Test of DE-O Method

Tolerance	ρ	Avg (Max) FEs	RMSE	Max Abs Error	Options/Sec
1.E-10	All ρ	314 (2,746)	4.5E-05	1.2E-02	9,566
1.E-10	$\rho = 0$	294 (990)	3.2E-05	4.3E-03	15,354
1.E-12	All ρ	364 (3,312)	6.0E-07	3.0E-04	8,168
1.E-12	$\rho = 0$	337 (1,050)	4.7E-12	4.7E-10	13,490
1.E-14	All ρ	454 (3,884)	2.6E-06	9.6E-04	6,604
1.E-14	$\rho = 0$	404 (2,220)	1.8E-12	1.2E-10	11,095

Bulk test performance results for put option pricing with the DE-O method. For all cases we use the integrand (24) with $\alpha = -1/2$ and $\varphi = 0$ (see Section 5.2). Test cases cover the contract and model parameter ranges outlined in Section 6.1, with a carve-out of the set of scenarios for which the correlation equals zero ("$\rho = 0$"). The "Tolerance" column is the *requested* absolute tolerance for the adaptive quadrature. Other columns are as in Tables 1 and 3, except for the fact that all errors are expressed in absolute, rather than relative, terms. The benchmark used for empirical error analysis was the DE-C method with a relative tolerance of 10^{-15}.

For the case $\rho = 0$, the DE-O method is quite efficient, and offers a good alternative to the DE-C scheme, especially for users that either do not want to work in complex arithmetic or do not wish to make the changes to the integrand that are needed to work with an angled contour. For the general case, the DE-O results are generally less attractive than those of the DE-C method, although still quite respectable (keeping in mind that the reference level for F, K is 100). While the Ooura method is popular in the scientific community for its good "out-of-the-box" performance, for the specific application in this paper the more targeted approach in the DE-C method is superior.

7 Conclusion

This paper has introduced a number of different techniques to improve numerical efficiency and robustness in option pricing based on Fourier integrations of a characteristic function. Overall, the best-performing technique involved an angled straight-line contour path in the complex plane, coupled with either automatic or fixed double-exponential quadrature. We tested both exp-sinh and tanh-sinh double-exponential mappings, and found both to strongly outperform a variety of standard methods. For instance, we experienced significant improvements in robustness accompanied by precision improvement of many (typically 10 or more) orders of magnitude when comparing to the standard adaptive Gauss-Lobatto quadrature. A specialized double-exponential method based on the node placement trick of [49] and [50] offered a reasonable, but

overall inferior, alternative to those that prefer not to alter the integration path, especially for the practically relevant case of zero correlation, $\rho = 0$.

For concreteness, we limited ourselves to the Heston model setting, which is both particularly popular in practice and particularly challenging numerically. Applications of DE quadrature and/or angled contour integration to other models, such as those in the Levy class, are straightforward. We leave numerical experiments on such models to future research, but can safely predict that the introduction of an angled integration path, whenever possible, will lead to efficiency gains, irrespective of which quadrature rule is ultimately used.

Finally, we note that our choice of a straight-line contour integral with (essentially) parameter-invariant magnitude of the slope in the complex plane (see (25)) was done mostly for simplicity and ease of implementation. One could, however, easily imagine that more sophisticated choices of slope could lead to even better results. More generally, the result in our Proposition 1 will apply to a wide variety of curves in the complex plane, and it is likely that even more performant non-linear contour paths can be constructed, in a model-specific manner. This interesting idea is another possible topic for future research.

A Appendix: Implementing the Characteristic Function

In any direct integration method for the Heston model the bulk of the computation time is going to be spent in evaluating ϕ_H. An implementation should make sure this evaluation is fast and accurate, so we here list (in Algorithm 1 below) a concrete calculation sequence that aims to reduce cancellation errors. We have assumed the availability of the functions

$$\mathrm{expm1}(z) = e^z - 1, \qquad \mathrm{log1p}(z) = \ln(1+z).$$

For real arguments these functions are provided by many languages; for instance, the C++ Standard Library has made them available since C++11. For complex arguments, $z = a + ib$, we can use the real versions along with

$$\mathrm{cosm1}(b) = \cos(b) - 1 = -2\sin^2(b/2),$$

$$\mathrm{expm1}(z) = \begin{cases} (\mathrm{expm1}(a)\cdot\mathrm{cosm1}(b) + \mathrm{expm1}(a) + \mathrm{cosm1}(b)) + i\sin(b)\exp(a), & |z| < 1, \\ \exp(z) - 1, & \text{otherwise}, \end{cases}$$

$$\mathrm{log1p}(z) = \begin{cases} \frac{1}{2}\mathrm{log1p}(a^2 + 2a + b^2) + i\arg(1+z), & |a|, |b| < \frac{1}{2}, \\ \ln(1+z), & \text{otherwise}. \end{cases}$$

Algorithm 1 Heston Characteristic Function.

procedure HESTONPHI(u)
  if $\mathrm{Re}\{\beta\} \cdot \mathrm{Re}\{D\} + \mathrm{Im}\{\beta\} \cdot \mathrm{Im}\{D\} > 0$ **then**
    $r \leftarrow -\epsilon^2 u(u+i)/(\beta + D)$
  else
    $r \leftarrow \beta - D$
  end if
  if $D \neq 0$ **then**
    $y \leftarrow \mathrm{expm1}(-DT)/2D$
  else
    $y \leftarrow -T/2$
  end if
  $A \leftarrow (\kappa\theta/\epsilon^2)(rT - 2\log 1\mathrm{p}(-ry))$
  $B \leftarrow u(u+i)y/(1-ry)$
  return $\exp(A + v_0 B)$
end procedure

B Appendix: Locating $\alpha_{\min}$ and $\alpha_{\max}$

As we do not have closed-form expressions for $\alpha_{\min}$ and $\alpha_{\max}$, we have to compute them numerically using a root-search algorithm[18]. Application of numerical root search will require bounds bracketing $\alpha_{\min}$ and $\alpha_{\max}$, a problem that we address in this appendix.

It is convenient to work with $k = \alpha + 1$, so we focus on bracketing $k_{\min}$ and $k_{\max}$, where $k_{\min} = \alpha_{\min}+1$ and $k_{\max} = \alpha_{\max}+1$. To proceed, we need some additional notation. First, recall the functions β, D from (9) for which

$$\beta(-ki) = \kappa - \rho\epsilon k, \qquad D^2(-ki) = \beta^2(-ki) - \epsilon^2 k(k-1).$$

We suppress the argument $-ki$ when it is clear from the context. Let also

$$k_\pm(x) = \frac{(\epsilon - 2\rho\kappa) \pm \sqrt{(\epsilon - 2\rho\kappa)^2 + 4(\kappa^2 + x^2/T^2)(1-\rho^2)}}{2\epsilon(1-\rho^2)}$$

be the roots of the quadratic $D^2 = -x^2/T^2$, with

$$k_\pm \triangleq k_\pm(0).$$

D is real for $k \in [k_-, k_+]$ and pure imaginary otherwise.

Now, the singularities of ϕ_H occur at points $-ki$, where k is any moment of X that explodes. Using a result of [4] (Proposition 3.1 and Remark 3.1), we can express these

[18] We use a modified *regula falsi* method. This has super-linear convergence, is derivative-free, and keeps the root bracketed.

critical moments as the solutions of $M(k) = T$ where

$$M(k) = \begin{cases} \frac{1}{D} \ln\left(\frac{\beta - D}{\beta + D}\right), & k \in [k_-, k_+], \\ \frac{2}{|D|}\left(\pi \cdot 1_{\beta>0} - \arctan\left(\frac{|D|}{\beta}\right)\right), & k \notin [k_-, k_+]. \end{cases} \tag{36}$$

Remark 1 *Alternatively, following [52], the critical moments are the roots of*

$$F(k) = \begin{cases} \cosh(DT/2) + \beta \sinh(DT/2)/D, & k \in [k_-, k_+], \\ \cos(|D|T/2) + \beta \sin(|D|T/2)/|D|, & k \notin [k_-, k_+]. \end{cases} \tag{37}$$

The formulations are equivalent; the formulation in [4] is somewhat preferable in the implementation as there are fewer transcendental function calls. However, the [52] formulation may simplify theoretical analysis.

Let us note the following symmetry result:

Lemma 2 *Let $\bar{\kappa} = \kappa - \rho\epsilon > 0$, $\bar{\rho} = -\rho$, and $\bar{\epsilon} = \epsilon$. Also let $\bar{k}_{min}, \bar{k}_{max}$ be the counterparts of k_{min}, k_{max} for the Heston process with parameters $\bar{\kappa}$, $\bar{\rho}$, and $\bar{\epsilon}$ replacing κ, ρ, and ϵ respectively. Then, $\bar{k}_{min} = 1 - k_{max}$ and $\bar{k}_{max} = 1 - k_{min}$.*

Proof: It is easy to check that

$$\bar{\beta}(-ki) \triangleq \bar{\kappa} - \bar{\rho}\bar{\epsilon}k = \beta(-(1-k)i),$$
$$\bar{D}^2(-ki) \triangleq \bar{\beta}^2(-ki) - \bar{\epsilon}^2 k(k-1) = \bar{D}^2(-(1-k)i).$$

Since the values of F only depend on the Heston parameters through β and D the result follows immediately. ∎

The key result for bracketing of $k_{\min}$ and $k_{\max}$, is given in [52] (Theorem 3.4, with a few minor corrections):

Proposition 2 (Rollin et al.) *Let $M(k)$ be defined as in (36). Then,*

1. *k_{min} is bracketed by $(k_-(2\pi), k_-)$. Also, $k_- < 0$.*
2. *If $\kappa - \rho\epsilon > 0$, k_{max} is bracketed by $(k_+, k_+(2\pi))$. Also, $k_+ > 1$.*
3. *If $\kappa - \rho\epsilon < 0$, let $T_{cut} = -2/(\kappa - \rho\epsilon k_+)$. Then*
   (a) *if $T < T_{cut}$, k_{max} is bracketed by $(k_+, k_+(\pi))$.*
   (b) *if $T \geq T_{cut}$, k_{max} is bracketed by $(1, k_+]$.*
4. *If $\kappa - \rho\epsilon = 0$, k_{max} = is bracketed by $(k_+, k_+(\pi))$. Also, $k_+ = 1$.*

Proof: See [52], except for Case 4 [19] which follows from checking that when $\kappa = \rho\epsilon$, F is monotonic and changes sign on $(1, k_+(\pi))$. [F is defined by (37).] [20] □

Using the result of Proposition 2, in all cases $k_{\min}$ and $k_{\max}$ can be determined by numerically solving $M(k) = T$ on the bracketing interval given in the proposition.

[19] In [52], the result for this case is incorrectly stated to be $k_{\max} = 1$.
[20] Case 2 also follows immediately from Case 1 and Lemma 2.

C Appendix: Implementing Ooura's Method

For t near 0, the expression for $g'(t)$ obtained by direct differentiation is subject to cancellation near the origin[21]. However, as we only need values at $0, \pm h, \pm 2h, \ldots, \ldots$, the value of h would need to be pathologically small to cause a major problem. Still, for reasonable h we might lose some significant digits, and it is preferable to avoid this. We here discuss a remedy from [11].

For $|t| < 1$, define the functions

$$e_1(t) = \frac{e^t - 1}{t}, \quad e_2(t) = \frac{e_1(t) - 1}{t}, \quad \upsilon(t) = 2 + \alpha e_1(-t) + \beta e_1(t).$$

Note that $e_1'(t) = e_1(t) - e_2(t)$. We can now write

$$g(t) = \frac{1}{\upsilon(t) e_1(-t\upsilon(t))}$$

and use logarithmic differentiation to get

$$g'(t) = g(t) \cdot (\ln g(t))' = g(t) \left(-\frac{\upsilon'(t)}{\upsilon(t)} + (\upsilon(t) + t\upsilon'(t)) \frac{e_1(-t\upsilon(t)) - e_2(-t\upsilon(t))}{e_1(-t\upsilon(t))} \right)$$

which is stable as long as we can evaluate $e_1(t), e_2(t)$ accurately for small t. The simplest way to do this is to use the Taylor expansion for $e_2(t)$ and then use $e_1(t) = 1 + te_2(t)$.

It is a good idea to avoid evaluating the trigonometric functions at large arguments. Noting the form of $g(t) = t/(1 - d(t))$ and applying some elementary identities we get

$$\sin\left(\frac{\pi}{2h}(g(nh) - nh)\right) \exp\left(\frac{i\pi}{2h}(g(nh) + nh)\right) =$$
$$\begin{cases} \sin\theta_n \cos\theta_n - i\cos^2\theta_n, & n \le 0 \text{ odd}, \\ \sin\theta_n \cos\theta_n + i\sin^2\theta_n, & n \le 0 \text{ even}, \\ (-1)^n(\sin\theta_n d_n \cos\theta_n d_n + i\sin^2\theta_n d_n), & n > 0, \end{cases}$$

where

$$\theta_n = \frac{\pi}{2h} g(nh),$$

and

$$d_n = \exp\left(-2nh - \alpha(1 - e^{-nh}) - \beta(e^{nh} - 1)\right) < 1$$

decays rapidly to zero.

[21] $g(t)$ can be evaluated using the function expm1 listed in Appendix A above.

References

[1] Albrecher, H., P. Mayer, W. Schoutens, and J. Tistaert (2007), "The Little Heston Trap," *Wilmott Magazine*, January, 83-92.

[2] Andersen, L. (2007), "Simple and Efficient Simulation of the Heston Stochastic Volatility Model," *Journal of Computational Finance*, 11, 1-42.

[3] Andersen, L. and J. Andreasen (2002), "Volatile Volatilities," *Risk Magazine*, December, 163-168.

[4] Andersen, L. and V. Piterbarg (2007), "Moment Explosions in Stochastic Volatility Models," *Finance and Stochastics*, 11(1), 29-50.

[5] Andersen, L. and V. Piterbarg (2010), *Interest Rate Modeling*, Vol. 1, Atlantic Financial Press.

[6] Andersen, L. and A. Lipton (2013), "Asymptotics for Exponential LÃ©vy Processes and Their Volatility Smile: Survey and New Results," *International Journal of Theoretical and Applied Finance*.

[7] Andersen, L., M. Lake, and D. Offengenden (2016), "High-Performance American Option Pricing," *Journal of Computational Finance,* 20 (1), 39-87.

[8] Bailey, D., X. Li, and K. Jeyabalan (2005), "A Comparison of Three High-Precision Quadrature Schemes," *Experimental Mathematics*, 14(3), 317–329.

[9] Barndorff-Nielsen, O. (1998), "Processes of the Normal Inverse Gaussian Type," *Finance and Stochastics*, 2, 41-68.

[10] Bates, D. (1996), "Jumps and Stochastic Volatility: Exchange Rate Processes implicit in Deutsche Mark Options," *Review of Financial Studies*, 9(1), 69-107.

[11] Bornemann, F., Laurie, D., Wagon, S., and Waldvogel, J. (2004), "The SIAM 100-digit challenge: a study in high-accuracy numerical computing (Vol. 86)," *SIAM*.

[12] Broadie, M. and Y. Yamamoto (2005), "A Double-Exponential Fast Gauss Transform Algorithm for Pricing Discrete Path-Dependent Options," *Operations Research*, 53(5), 764–779.

[13] Carr, P. and D. Madan (1999), "Option Valuation using the Fast Fourier Transform," *Journal of Computational Finance*, 2(4), 61-73.

[14] Carr, P., H. Geman, D. Madan, and M. Yor (2003), "The fine Structure of Asset Returns: an Empirical Investigation," *Journal of Business*, 75(2), 305-332.

[15] Carr, P. and L. Wu (2003), "The Finite Moment Log Stable Process and Option Pricing," *Journal of Finance*, 58(2), 753-777.

[16] Cheng, P. and O. Scaillet (2007), "Linear-Quadratic Jump-Diffusion Modeling," *Mathematical Finance*, 17(4).

[17] Chourdakis, K. (2005), "Option Pricing using the Fractional FFT," *Journal of Computational Finance*, 8(2), 1-18.

[18] Christoffersen, P., S. Heston, and K. Jacobs (2009), "The Shape and Term Structure of the Index Option Smirk: Why Multi-Factor Stochastic Volatility Models work so well," *Management Science*, 55(12), 1914-1932.

[19] Cont, R. and P. Tankov (2004), *Financial Modeling with Jump Processes*, Chapman & Hall.

[20] Dickinson, A. (2011), "Numerical Approximation of Option Premia in Displaced-Lognormal Heston Models," Working Paper, Bank of America Merrill Lynch.

[21] Duffie, D., J. Pan, and K. Singleton (2000), "Transform Analysis and Asset Pricing for Affine Jump-Diffusions," *Econometrica*, 68, 1343-1376.

[22] Fang, F. and C. Osterlee (2008), "A Novel Pricing Method for European Options based on Fourier-Cosine Series Expansions," *SIAM Journal of Scientific Computing*, 31(2), 1914-1932.

[23] Filon, L. (1928), "On a Quadrature Formula for Trigonometric Integrals," In: *Proceedings of the Royal Society Edinburgh*, 49, 38-47.

[24] Gander, W., and Gautschi, W. (2000), "Adaptive quadratureâ€"revisited, " *BIT Numerical Mathematics*, 40(1), 84-101.

[25] Gil-Pelaez, J. (1951), "Note on the Inversion Theorem," *Biometrika*, 38(3-4), 481â€"482.

[26] Glasserman, P., P. Heidelberger and P. Shahabuddin, "Portfolio Value-at-Risk with Heavy-Tailed Risk Factors," *Mathematical Finance*, 12, 239-269.

[27] Heston, S. (1993), "A closed-form Solution for Options with Stochastic Volatility and Applications to Bond and Currency Options," *Review of Financial Studies*, 6(2), 327-343.

[28] Huybrechs, D. and S. Vandewalle (2006), "On the Evaluation of Highly Oscillatory Integrals by Analytic Continuation," *SIAM Journal of Numerical Analysis*, 44 (3), 1026-1048.

[29] Jacquier, A. and C. Martini, "Heston 2010," Working Paper, Imperial College London.

[30] Joshi, M. and C. Yang (2011), "Fourier Transforms, Option Pricing and Controls," Working Paper, University of Melbourne.

[31] Kilin, F. (2011), "Accelerating the Calibration of Stochastic Volatility Models," *Journal of Derivatives*, 18(3), 7-16.

[32] Lee, R. (2005), "Option Pricing by Transform Methods: Extension, Unification, and Error Control," *Journal of Computational Finance*, 7(3), 51-86.

[33] Le Floc'h, F. (2016), "An adpative Filon quadrature for Stochastic Volatility Models," Working Paper.

[34] Le Floc'h, F. (2014), "Fourier Integration and Stochastic Volatility Calibration," Working Paper, Calypso Technology.

[35] Levin, D.(1995), "Fast Integration of Rapidly Oscillatory Functions, " *Journal of Computational and Applied Mathematics*, 63, 95-101.

[36] Lewis, A., (2000), *Option Valuation under Stochastic Volatility*, Finance Press, London.

[37] Lewis, A. (2001), "A Simple Option Formula for General Jump-Diffusion and other Exponential Levy Processes," Working Paper, OptionCity.net.

[38] Lipton, A. (2002), "The Vol Smile Problem," Risk Magazine, February, 61-65.

[39] R. Lord and C. Kahl (2007), "Optimal Fourier Inversion in Semi-Analytical Option Pricing," *Journal of Computational Finance*, 10(4), 1-30.

[40] R. Lord and C. Kahl (2010), "Complex Logarithms in Heston-Like Models," *Mathematical Finance*, 20(4), 671 - 694.

[41] Lucic, V. (2015), "On Singularities in the Heston Model," In: Friz, P., J. Gatheral, A. Gulisashvili, A. Jacquier, and J. Teichmann (eds.) *Large Deviations and Asymptotic Methods in Finance*, Springer Verlag.

[42] Madan, D., P. Carr, and E. Chang (1998), "The Variance Gamma Process and Option Pricing," *European Finance Review*, 2, 79-105.

[43] Matsuda, K. (2004), "Introduction to Option Pricing with Fourier Transform," Working Paper, City University of New York.

[44] Michalski, K. A., and Mosig, J. R. (2016), "Efficient Computation of Sommerfeld Integral Tails – Methods and Algorithms, " *Journal of Electromagnetic Waves and Applications*, 30(3), 281-317.

[45] Muhammad, M., and Mori, M. (2003). "Double exponential formulas for numerical indefinite integration, " *Journal of Computational and Applied Mathematics*, 161(2), 431-448.

[46] Mori, M. (1985), "Quadrature Formulas Obtained by Variable Transformation and the DE-Rule," *Journal of Comput. Appl. Math.*, 12 & 13, 119-130.

[47] Mori, M. and M. Sugihara (2001), "The Double-Exponential Transformation in Numerical Analysis," *Journal of Computational and Applied Mathematics*, 127(1), 287–296.

[48] Ooura, T. and M. Mori (1991), "The Double-Exponential Formula for Oscillatory Functions over the Half-Infinite Interval," *Journal of Computational and Applied Mathematics*, 38(1-3), 353-360.

[49] Ooura, T. and M. Mori (1999), "A Robust Double-Exponential Formula for Fourier-Type Integrals," *Journal of Computational and Applied Mathematics*, 112(1), 229-241.

[50] Ooura, T. (2005), "A Double-Exponential Formula for the Fourier Transform," *Publ. RIMS, Kyoto University,* 41(4), 971–977.

[51] Press, W., S. Teukolsky, W. Vetterling, and B. Flannery (2007), *Numerical Recipes: the Art of Scientific Computing*, 3rd ed., Cambridge University Press.

[52] Rollin, S., A. Ferreiro-Castilla, and F. Utzet (2009), "A new Look at the Heston Characteristic Function," *arXiv preprint arXiv:0902.2154*.

[53] Rouah, F. (2013), *The Heston Model and Its Extensions in Matlab and C#*, Wiley.

[54] Rouvinez, C. (1997), "Going Greek with VAR," *Risk Magazine*, 10(2), 57-65.

[55] Schmelzle, M. (2010), "Option Pricing Formulae using Fourier Transform: Theory and Application," Working Paper, pfadintegral.com.

[56] Schobel, R. and J. Zhu (1999), "Stochastic Volatility with an Ornstein-Uhlenbeck Process: An Extension," *European Finance Review*, 3, 23-46.

[57] Staunton, M. (2006), "Stochastic Volatility without Complex Numbers," *Wilmott Magazine*, May, 46-48.

[58] Stein, E. and J. Stein (1991), "Stock Pricing distribution with stochastic volatility," *Review of Financial Studies*, 4, 727-752.

[59] Sugihara, M. (1997), "Optimality of the Double Exponential Formula – Functional Analysis Approach," *Numerische Mathematik*, 75(3), 379–395.

[60] Takahasi, H. and M. Mori (1974), "Double Exponential Formulas for Numerical Integration," *Publ. RIMS, Kyoto University,* 9, 721-741.

[61] Titmarsch, E. (1975), *Introduction to the Theory of Fourier Integrals*, Reprint of 2nd ed., Oxford University Press, London.

[62] Trefethen, L. and J. Weideman (2014), "The Exponentially Convergent Trapezoidal Rule," *SIAM REVIEW*, 56(3), 385–458.

[63] Veberic, D. (2010), "Having fun with Lambert W(x) function," *arXiv preprint arXiv:1003.1628*.

[64] Ye, L. (2006), *Numerical Quadrature: Theory and Computation*, M.Sc. Thesis, Dahlhousie University.

[65] Zhu, J. (2010), *Applications of Fourier Transform Techniques to Smile Modeling*, 2nd ed., Springer, New York.